

Quantitative Quasiperiodicity

Suddhasattwa Das* Yoshitaka Saiki† Evelyn Sander§ James A Yorke‡

August 4, 2015

Abstract

The Birkhoff Ergodic Theorem concludes that time averages, that is, Birkhoff averages, $\Sigma_{n=1}^N f(x_n)/N$ of a function f along an ergodic trajectory (x_n) of a function T converges to the space average $\int f d\mu$, where μ is the unique invariant probability measure. Convergence of the time average to the space average is slow. We introduce a modified average of $f(x_n)$ by giving very small weights to the “end” terms when n is near 0 or N . When (x_n) is a trajectory on a quasiperiodic torus and f and T are C^∞ , we show that our weighted Birkhoff averages converge “super” fast to $\int f d\mu$, *i.e.* with error smaller than every polynomial of $1/N$. Our goal is to show that our weighted Birkhoff average is a powerful computational tool, and this paper illustrates its use for several examples where the quasiperiodic set is one or two dimensional. In particular, we compute rotation numbers and conjugacies (*i.e.* changes of variables) and their Fourier series, often with 30-digit precision.

Introduction

Quasiperiodicity is a key type of observed dynamical behavior in a diverse set of applications. Tori with quasiperiodic motion persist for small perturbations by the Kolmogorov-Arnold-Moser theory, but such behavior is also observed for non-conservative systems well beyond this restricted regime. We believe that quasiperiodicity is one of only three types of dynamical behaviors occurring in basic sets of typical systems. See [1] for the statement of our formal conjecture of this basic set triumvirate. For example, quasiperiodicity occurs in a system of weakly coupled oscillators, in which there is an invariant smooth attracting torus in phase space with behavior described exclusively by the phase angles of rotation of the system. Indeed, it is the property of the motion being described using only a set of phase angles that always characterizes quasiperiodic behavior. In a now classical set of papers, Newhouse, Ruelle, and Takens demonstrated a route to chaos through a region with quasiperiodic behavior, causing a surge in the study of the motion [2]. There is active current interest in development of a systematic numerical and theoretical approach to bifurcation theory for quasiperiodic systems.

Our goal in this paper is to present a fast numerical method for the fast calculation of the limit of Birkhoff averages in quasiperiodic systems, allowing us to compute various key quantities. If f is integrable and the dynamical system is ergodic on the set in which the trajectory lives, then the Birkhoff Ergodic Theorem asserts that the Birkhoff average $\Sigma_{n=1}^N f(x_n)/N$ of a function f along an ergodic trajectory (x_n) converges to the space average $\int f d\mu$ as $N \rightarrow \infty$ for μ -almost every x_0 , where μ is the unique invariant probability measure. We develop a numerical method for calculating the limit of such averages, where instead of weighting the terms $f(x_n)$ in the average equally, we weight the early and late terms

*Department of Mathematics, University of Maryland, College Park

†Graduate School of Commerce and Management, Hitotsubashi University

‡University of Maryland, College Park

§Department of Mathematical Sciences, George Mason University

of the set $\{1, \dots, N\}$ much less than the terms with $n \sim N/2$ in the middle. That is, rather than using the equal weighting $(1/N)$ in the Birkhoff average, we use a weighting function $w(n/N)$, which will primarily be the following well known C^∞ function that we will call the **exponential weighting function**, $w_{\text{exp}}(t) = \exp(1/(t(t-1)))$. In a companion paper [3], it is rigorously shown that for quasiperiodic systems and $C^\infty f$, this weighting function leads to super convergence with respect to N , meaning faster than any polynomial in N^{-1} . This super convergence arises from the fact that we are taking advantage of the quasiperiodic nature of the map or flow. In particular, our method uses the underlying structure of a quasiperiodic system, and would not give improved convergence results for chaotic systems. We demonstrate the method and its convergence rate by computing rotation numbers, conjugacies, and their Fourier series in dimensions one and two. We will refer to a 1D quasiperiodic curve as a (*topological*) *circle*.

Other authors have considered related numerical methods before, in particular [4, 5], which we will compare to when we introduce our method. See also [6, 7, 8, 9, 10, 11, 12, 13, 14, 15].

Our paper proceeds as follows: In Section 2, we give the formal definition of quasiperiodicity, rotation, and the conjugacy map. In Section 3.1, we describe our numerical method in detail. We illustrate our method for a series of four examples, including an example of a two-dimensionally quasiperiodic map. In all cases, we get fast convergence and are in most cases able to give results with thirty digits of precision. For convenience of the reader, have summarized our numerical findings in Table 1.

We start by describing our results for a key example of quasiperiodicity: the (circular) restricted three-body problem. This is an idealized model of the motion of the planet, a large moon, and a spacecraft governed by Newtonian mechanics, in a model studied by Poincaré [16, 17]. In particular, we consider a planar three-body problem consisting of two massive bodies (“planet” and “moon”) moving in circles about their center of mass and a third body (“spacecraft”) whose mass is infinitesimal, having no effect on the dynamics of the other two.

We assume that the moon has mass μ and the planet mass is $1 - \mu$ where $\mu = 0.1$, and writing equations in rotating coordinates around the center of mass. Thus the planet remains fixed at $(-0.1, 0)$, and the moon is fixed at $(0.9, 0)$. In these coordinates, the satellite’s location and velocity are given by the *generalized position vector* (q_1, q_2) and *generalized velocity vector* (p_1, p_2) . The equations of motion are as follows (see [17]).

$$\begin{aligned} dq_1/dt &= p_1 + q_2, \\ dq_2/dt &= p_2 - q_1, \\ dp_1/dt &= p_2 - \mu(q_1 - 1 + \rho)d_{\text{moon}}^{-3} - (1 - \mu)(q_1 + \mu)d_{\text{planet}}^{-3}, \\ dp_2/dt &= -p_1 - \mu q_2 d_{\text{moon}}^{-3} - (1 - \mu)q_2 d_{\text{planet}}^{-3}, \end{aligned} \tag{1}$$

where

$$d_{\text{moon}} = ((q_1 - 1 + \mu)^2 + q_2^2)^{0.5} \text{ and } d_{\text{planet}} = ((q_1 + \mu)^2 + q_2^2)^{0.5}.$$

The following function H is a Hamiltonian for this system

$$H = [(p_1^2 + p_2^2)/2] + [q_2 p_1 - q_1 p_2] - [\mu d_{\text{planet}}^{-1} + (1 - \mu) d_{\text{moon}}^{-1}]. \tag{2}$$

The terms in the square brackets are resp. the kinetic energy, angular momentum and the angular potential. For fixed H , Poincaré reduced this problem to the study of the Poincaré return map for a fixed value of H , only considering a discrete trajectory of the values of (q_1, p_1) on the section $q_2 = 0$ and $\frac{dq_2}{dt} > 0$. Thus we consider a map in two dimensions rather than a flow in four dimensions. Figure 2 shows one possible motion of the spacecraft for the full flow. The orbit is spiraling on a torus. The black circle shows the corresponding trajectory on the Poincaré return map. Fig. 1 shows the Poincaré return map for the spacecraft for a variety of starting points. A variety of orbits are shown, most of which are quasiperiodic invariant circles. An exception is A-trajectory in Fig. 1(a), which is an invariant recurrent set consisting of 42 circles. Each circle is an invariant quasiperiodic circle under the 42-nd iterate of the map. Using our

Example	Equation	Rotation number(s)	Related Figures
Restricted three-body problem	1	0.063961728757453097164077919081024	1, 3, 2
Standard map	12	0.12055272197375513300298164369839	4, 5
Forced van der Pol oscillator, $F = 5$	13	0.29206126329199589285577578718959	6
Forced van der Pol oscillator, $F = 15$	13	0.37553441113144010884908928083318	6
Forced van der Pol oscillator, $F = 25$	13	0.56235370092685056634419221336154	6
Two-dimensional torus	14	ρ_1, ρ_2 in Table 2	7, 9

Table 1: **Summary of our numerical calculations.**

numerical method for Birkhoff averages, in the itemized list given below we summarize our results for the quasiperiodic orbit labeled B_1 .

The error in the quasiperiodicity computations using weighted Birkhoff averages decreases exponentially in the number of iterates N (see Fig. 3c). This speed of convergence means the accuracy of our solutions is the limit of numeric precision. In particular, we have computed trajectories for the Poincaré return map using an 8-th order Runge-Kutta method with time step 10^{-5} , in quadruple precision, meaning our results given below are computed up to thirty digits of accuracy. Section 2 formally defines the computed values given in this list.

1. The rotation number is given in Table 1, computed to 30 digits of accuracy.
2. We can compute the Fourier series of up to 200 terms. There is a conjugacy map h between the first return map and a rigid rotation on the circle. Evaluating the Fourier series allows us to reconstruct the conjugacy map (*cf.* Fig. 3a).
3. The exponential decay of the coefficients in the Fourier series is a strong indication of the analyticity of conjugacy function (*cf.* Fig. 3b).

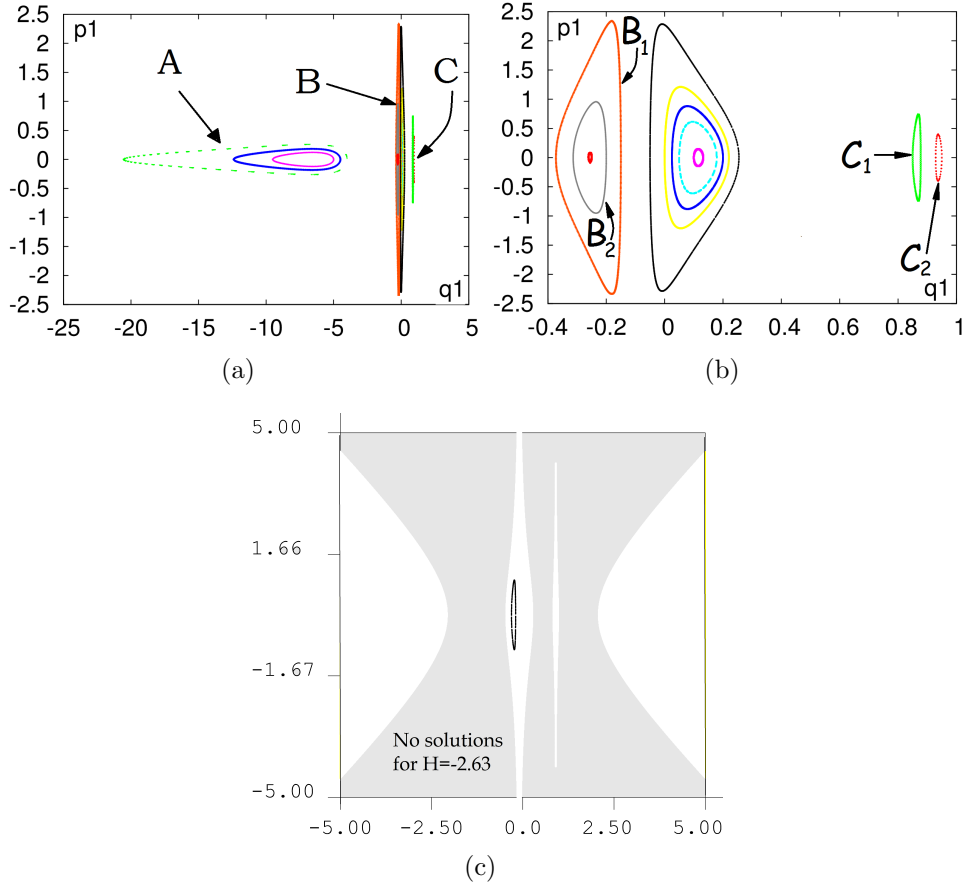
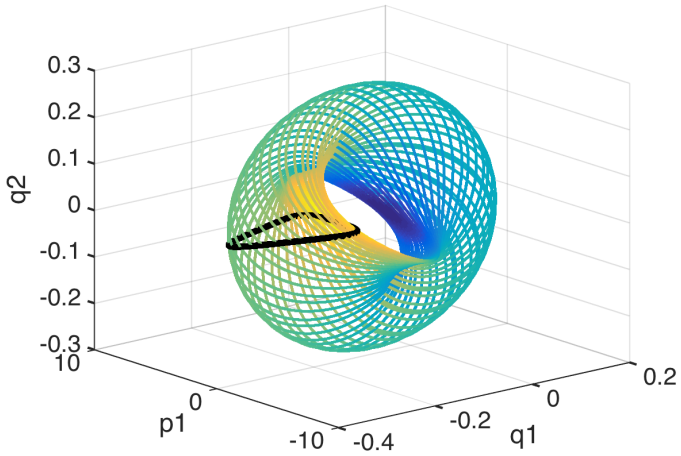
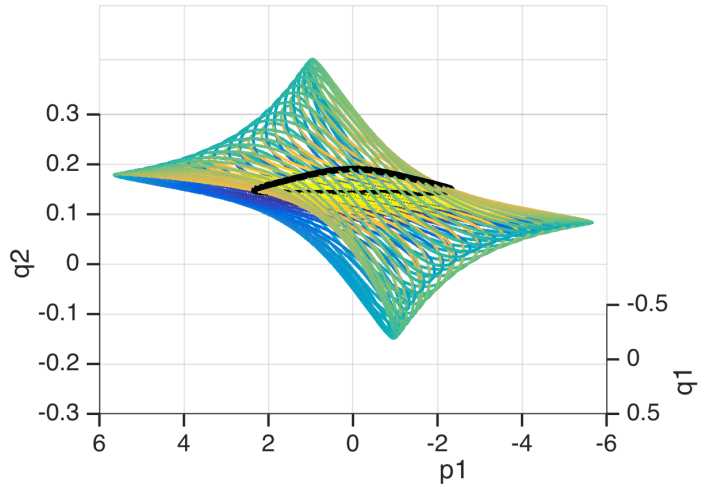


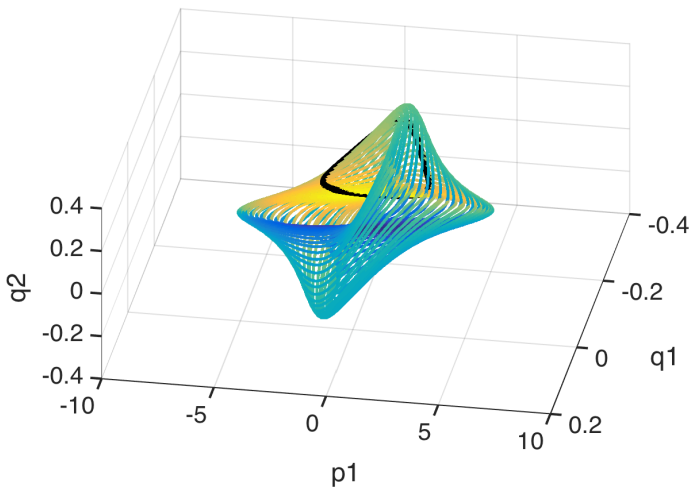
Figure 1: **Poincaré-return map for the restricted three-body problem.** All three parts show a projection to the $q_1 - p_1$ plane. Figures (a) and (b) show various quasiperiodic trajectories on the Poincaré section $q_2 = 0$, of the restricted three-body problem (1). Note that the planet is fixed at the point $(-0.1, 0)$ and the planet at $(0.9, 0)$. Thus some trajectories orbit both the planet-moon system and some only orbit the planet or the moon. Each time the flow hits $q_2 = 0$ and $\frac{dq_2}{dt} > 0$, we plot (q_1, p_1) . Each trajectory shown is a (topological) circle with quasiperiodic motion. The energy H for all the circles shown in the figures, including B_1 is the same and $H \approx -2.63$. Part (c) shows in white all the initial points (q_1, p_1) on the Poincaré surface for which there exists a p_2 so that the Hamiltonian H at $(q_1, q_2 = 0, p_1, p_2)$ is the same as the one in parts (a) and (b). Part (c) also shows the trajectory which corresponds to the circle B_1 in (a) and (b).



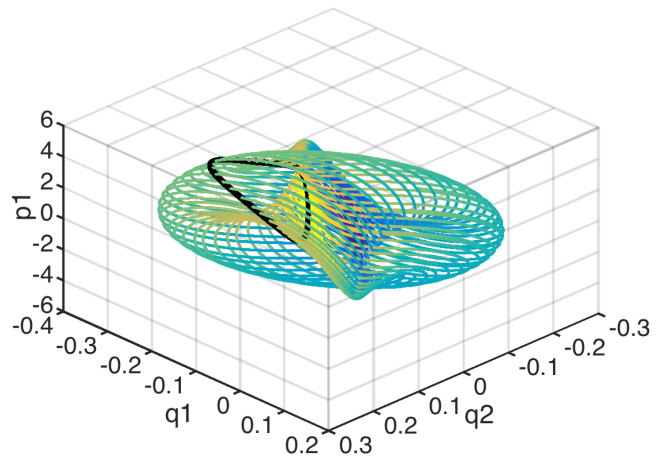
(a)



(b)



(c)



(d)

Figure 2: **Torus flow for the restricted three-body problem.** All four views are of the same two-dimensional quasiperiodic torus lying in \mathbb{R}^4 . Each picture consists of the same trajectory spiralling densely on this torus. This trajectory is the solution of (1), shown as curve B_1 in Fig. 1. We require four different views of this torus because the embedding into three dimensions gives a highly non-intuitive images. The black circle is the set of values of the Poincaré return map with $q_2 = 0$ for this flow torus.

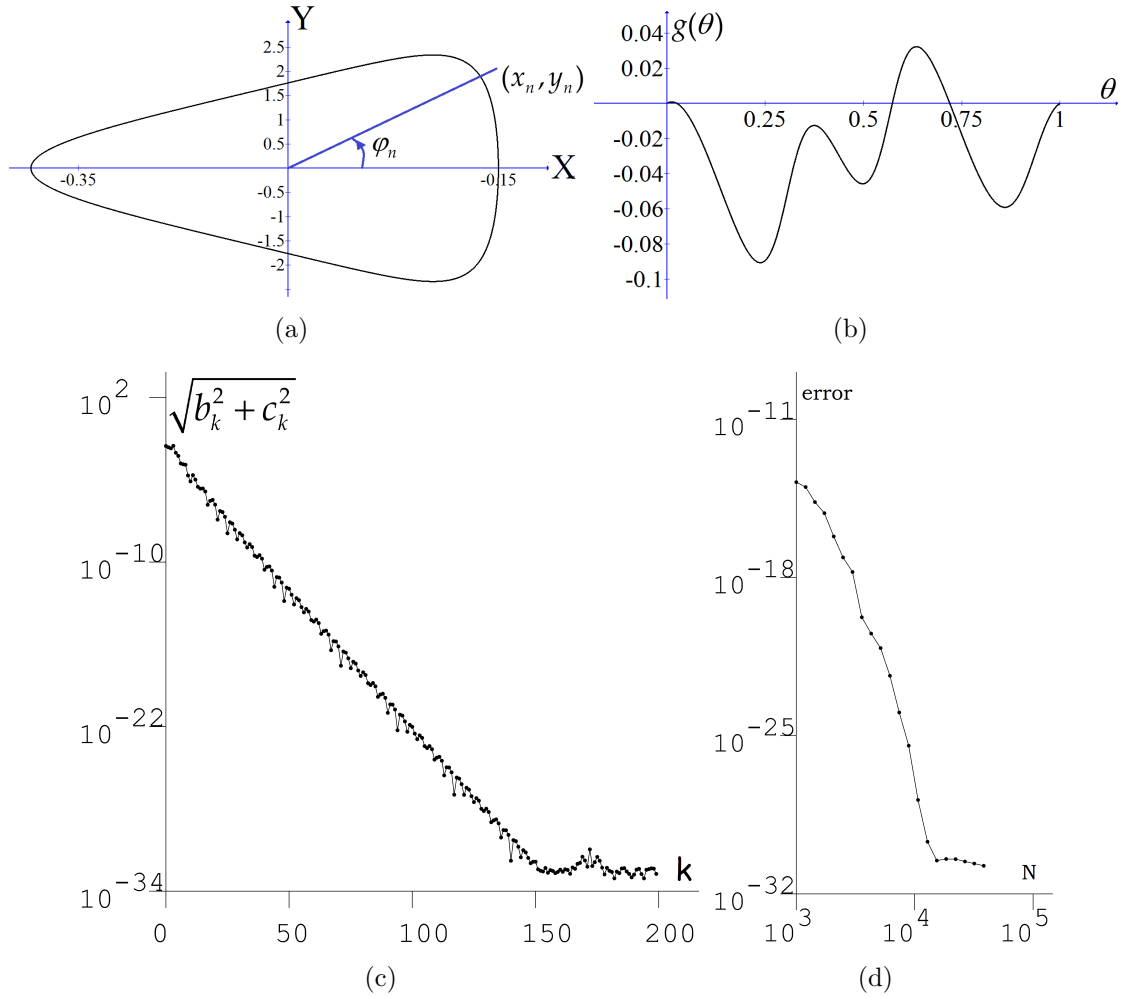


Figure 3: **Quasiperiodicity for the restricted three-body problem.** For the quasiperiodic circle B_1 in Fig. 1, Part(a) shows how the invariant circle is parameterized by coordinates $\phi \in S^1 \equiv [0, 1)$. Part (b) depicts the periodic part $g(\theta)$ of the conjugacy between the quasiperiodic behavior and rigid rotation by ρ . See (5) for a description of $g(\theta)$. Part (c) shows the norm of the Fourier coefficients of the conjugacy as a function of index. This exponential decay indicates that the conjugacy function is analytic, up to numerical precision. Part (d) shows the convergence rate of the error in the rotation number ρ_N as a function of the number of iterates N . The “error” is the difference $|\rho_N - \rho_{N^*}|$, where N^* is large enough so that ρ_N appears to have converged. The step size used for the Runge-Kutta (RK8) scheme is 10^{-5} .

2 Quasiperiodicity

In the introduction, we described quasiperiodic motion as motion that could be fully understood through a set of angles of rotation. We now formalize that idea in the following definition for quasiperiodicity.

Quasiperiodicity For a dimension $d \geq 1$, let $\rho = (\rho_1, \rho_2, \dots, \rho_d)$ be a rotation vector such that all ρ_k are irrational and irrationally related (defined below in (8)). Then following map is known as a **rigid irrational rotation**:

$$T_{\vec{\rho}}(\theta) = \theta + \rho \pmod{1}, \text{ where } 0 \leq \theta_k \leq 1, k = 1, 2, \dots, n. \quad (3)$$

A rigid rotation the simplest, albeit least interesting example of a map with quasiperiodicity. Since $T_{\vec{\rho}}$ gives the same values on opposite sides of the unit cube, we identify the sides and refer to the domain of the rigid rotation as a **circle** in one dimension and an **n -torus** in $n > 1$ dimension. From now on we will refer to the circle as a 1-torus. We define a general map T to be **quasiperiodic** if either T or some iterate T^k is topologically conjugate to a rigid rotation. (We will assume $k = 1$ in the rest of this description.) That is, a map T is quasiperiodic if there is a rigid rotation map $T_{\vec{\rho}}$ and an invertible **conjugacy map** h such that

$$T(h(\theta)) = h(T_{\vec{\rho}}(\theta)).$$

A flow has quasiperiodic behavior if its associated first return Poincaré map has quasiperiodic behavior.

Since we are focused on maps, we restate this definition in terms of iterates. Let (x_n) be the forward orbit under T , and (θ_n) the forward orbit under $T_{\vec{\rho}}$. That is, $x_{n+1} = T(x_n)$ and $\theta_{n+1} = \theta_n + \rho \pmod{1}$. Then as long as $\phi_0 = h(\theta_0) = h(0)$,

$$\phi_n = h(\theta_n) \text{ for all } n = 0, 1, 2, 3, \dots \quad (4)$$

The map h maps a torus to the domain of T , meaning that the domain of T is a topological circle or torus. Since h is a homeomorphism, the map

$$g(\theta) := h(\theta) - \theta \quad (5)$$

is periodic.

Thus a map T restricted to an invariant topological circle C is quasiperiodic if there is an continuous invertible map h from C to the true circle which maps T to a rigid irrational rotation map.

For an invertible map F to be quasiperiodic on a topological circle C , it is necessary and sufficient that F has a dense trajectory, as shown in [18]. In general, a circle homeomorphism without periodic points may not be quasiperiodic. However, if we assume that the map F and the topological circle C are twice continuously differentiable, then Denjoy [19] showed that these conditions are both necessary and sufficient. Furthermore, clearly any rigid irrational rotation map is a real analytic map, but even if we assume that a quasiperiodic function is analytic, Arnold showed that the conjugacy map h may only be continuous for some atypical rotation number. However, Herman (see [20]) proved that for circle homeomorphisms, most conjugacy maps h are analytic.

3 Our WB_{N+} method and its applications

3.1 Rotation number

Here is our method for calculating the limit of the Birkhoff average $\lim_{N \rightarrow \infty} \sum_{n=1}^N f(x_n)/N = \int f d\mu$ along an ergodic trajectory (or first return map) (x_n) . Let the weighting function w be defined as

$$w_{exp}(t) := w(t) := \begin{cases} \exp\left(\frac{1}{t(t-1)}\right), & \text{for } t \in (0, 1) \\ 0, & \text{for } t \notin (0, 1). \end{cases} \quad (6)$$

Let T be quasiperiodic on some set X_0 , with X_0 a topological torus. Henceforth, $X_0 \equiv \mathbb{T}^d$ will denote a d -dimensional topological torus. For $d = 1$, \mathbb{T}^d is a topological circle. For a continuous function f and a C^∞ quasiperiodic map T on \mathbb{T}^d , let $x_n \in \mathbb{T}^d$ be such that $x_n = T(x_{n-1})$ for all $n > 1$. We define a **Weighted Birkhoff** (WB_N) **average** of f as

$$\text{WB}_N(f)(x) := \sum_{n=0}^{N-1} \hat{w}_{n,N} f(x_n), \text{ where } \hat{w}_{n,N} = \frac{w(n/N)}{\sum_{j=0}^{N-1} w(j/N)} \quad (7)$$

In a companion paper [3], it is shown that if f and T are C^∞ , then for every positive integer m there is a constant $C_m > 0$ such that

$$\left| \text{WB}_N(f)(x) - \int f d\mu \right| \leq C_m N^{-m} \text{ for every } m.$$

We refer to the above as **super** (polynomial) **convergence** or **exponential convergence**.

Our numerical method converges fast enough to allow us to obtain high precision values for $\int f d\mu$ with relatively low computational cost. In particular, by appropriate choices for f , we obtain rotation numbers and sometimes the Lyapunov exponents, Fourier coefficients, and conjugacy reconstructions for quasiperiodic maps and flows potentially in any finite dimension, though here we work mainly in dimension one, with one example in dimension two. We now show how to apply this general method to computation of specific quantities. We observe that N must be larger for \mathbb{T}^2 than for \mathbb{T}^1 , to get a 30-digit accuracy.

Calculation of rotation vectors. Recall that every quasiperiodic map is conjugate to a pure rotation T_ρ by a vector $\rho = (\rho_1, \dots, \rho_n)$. In our discussion, we assume that the components of ρ are irrational and irrationally related. When we say that ρ_1, \dots, ρ_d are irrationally related, we mean that there are no integers k_1, \dots, k_d and k_0 for which,

$$k_1 \rho_1 + k_2 \rho_2 + \dots + k_d \rho_d \neq k_0 \quad (8)$$

unless all k_i are zero. Since we are only provided with the map T and not with the map R , we need a way of recovering this rotation vector using only a forward trajectory of the map T . The following formula gives a way of calculating the rotation vector ρ directly from the original map. The rotation vector given in the formula is valid well beyond the case of a quasiperiodic function. For example, the rotation vector can certainly be rational in one or all of its components.

Rotation vectors. Let $q(x) = x \pmod{1}$ and define $q: \mathbb{R}^d \rightarrow \mathbb{T}^d$ to be the projection map modulo \mathbb{Z} in each coordinate. For example, in one dimension the circle $[0, 1]$ with ends identified is the image of the real \mathbb{R} under the map q . For any homeomorphism $T: \mathbb{T}^d \rightarrow \mathbb{T}^d$, let $\bar{T}: \mathbb{R}^d \rightarrow \mathbb{R}^d$ be the lift of T . That is,

$$q \circ \bar{T} = \phi \circ q.$$

Since T is a homeomorphism, the map $\bar{T}(x) - x$ must be periodic in x with period 1. The rotation vector of a homeomorphism $T: \mathbb{T}^d \rightarrow \mathbb{T}^d$ starting at lift point z is given by

$$\rho(T, z) := \lim_{n \rightarrow \infty} \frac{\bar{T}^n(z) - z}{n}. \quad (9)$$

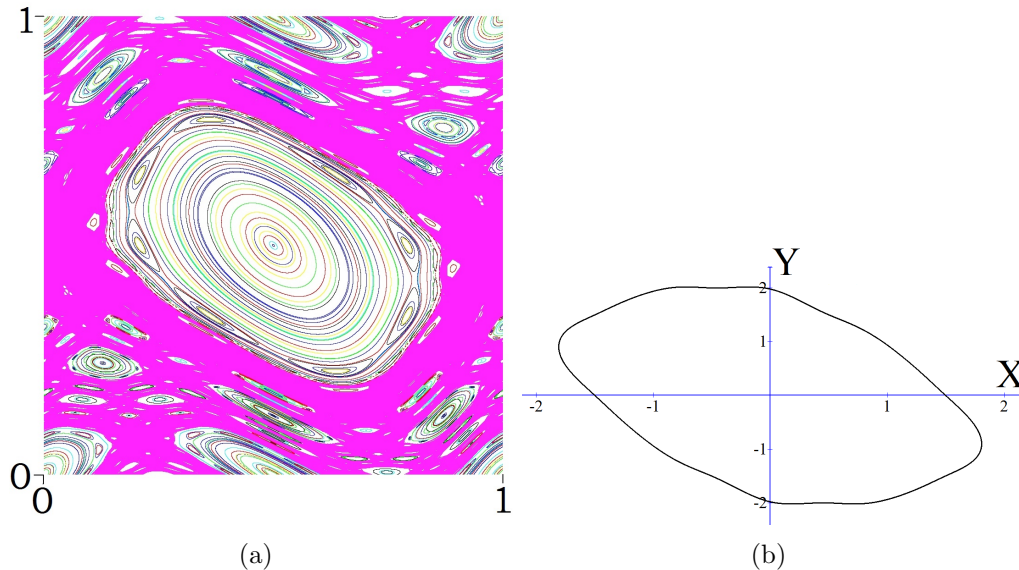


Figure 4: **The standard map.** A variety of orbits from different initial conditions in the standard map S_1 defined in (12) are plotted on the left. We can see both chaos (in pink) and quasiperiodic orbits under this map. A single topological circle with quasiperiodic behavior is plotted on the right. The orbit has initial conditions $(x, y) \approx (-0.607, 2.01)$. That is, if we restrict the map to this invariant circle, then it is topologically conjugate to a rigid irrational rotation.

Note that possible rotation numbers (ρ_1, ρ_2) of a quasiperiodic map on a torus \mathbb{T}^d depend on the coordinates chosen for T and z . For example, for domain \mathbb{T}^2 , the set of pairs (ρ_1, ρ_2) possible for a fixed T is dense in the two-torus. See [3].

Based on the above definition, the standard method of computing ρ from an orbit (y_k) of length n is to calculate the average

$$\rho \approx \frac{1}{N} \sum_{n=1}^N (\bar{T}(y_n) - y_n). \quad (10)$$

This method converges slowly at best, with order of only $1/N$ [4]. However, since Eq. 10 can be written as a Birkhoff average by writing $f(y_n) = T(y_n) - y_n$, we can apply our method to this function. That is, let $(y_k)_{k=0}^n$ be a forward orbit for \bar{T} . Our approximation of ρ is given by the weighted average of f ,

$$\text{WB}_N(y_{n+1} - y_n) := \sum_{n=0}^{N-1} \hat{w}_{n,N}(y_{n+1} - y_n) \rightarrow \rho. \quad (11)$$

Rotation number for the restricted three-body problem. In the introduction, we stated our results, including the rotation number for a quasiperiodic orbit for the restricted three-body problem. Fig. 3(b) shows the convergence rate of the calculation for this rotation number. .

Rotation number for the standard map. The standard map is an area preserving map on the two-dimensional torus, often studied as a typical example of analytic twist maps (see [21]). It is defined as follows*

$$S_1 \begin{pmatrix} x \\ y \end{pmatrix} = \begin{pmatrix} x + y \\ y + \sin x \end{pmatrix} \pmod{2\pi}. \quad (12)$$

The left-hand panel of Fig. 4 shows the trajectories starting at a variety of different initial conditions plotted in different colors. The shaded set is a large invariant chaotic set with chaotic behavior, but

*The standard map generally depends on a parameter α , but we only consider the case $\alpha = 1$.

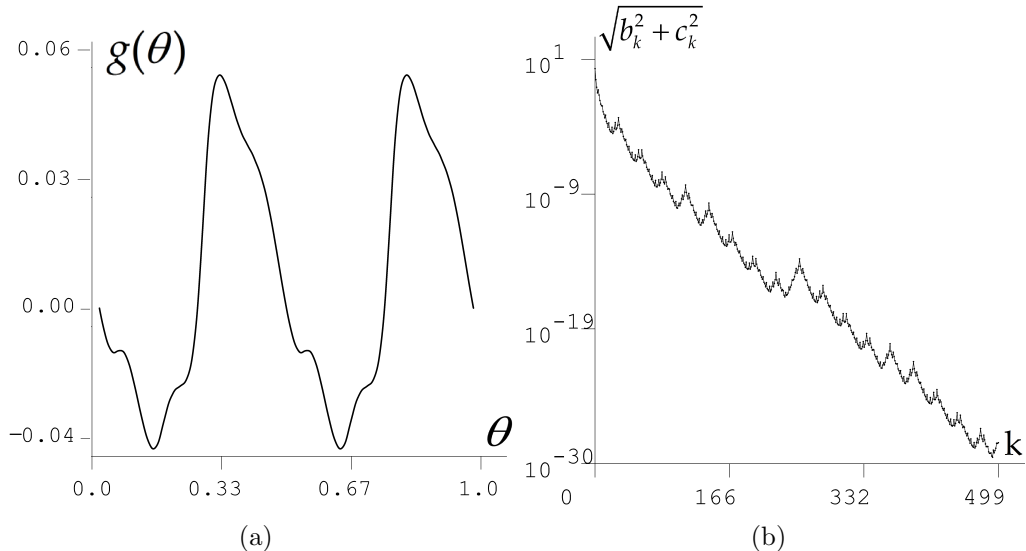


Figure 5: **The Standard map conjugacy.** Fig. (a) shows the change of variables which converts the motion on the circle in Fig. 4b into a pure rotation. Fig. (b) shows the decay of the Fourier coefficients. Since the conjugacy is an odd function, the odd-numbered Fourier sine and cosine terms are zero and therefore have been omitted from the picture. The decay of the Fourier terms can be bounded from above by an exponential decay, which suggests that the conjugacy is analytic.

many other invariant sets consist of one or more topological circles, on which the system has quasiperiodic behavior. For example, initial conditions $(\pi, 1.65)$ leads to chaos while $(\pi, 1.5)$ leads to a quasiperiodic trajectory. As is clearly the case here, one-dimensional quasiperiodic sets often occur in families for nonlinear processes, structured like the rings of an onion. There are typically narrow bands of chaos between quasiperiodic onion rings. Usually these inner rings are differentiable images of the n -torus, Yamaguchi and Tanikawa [21] and Chow et. al. in [22] showed that the outermost limit (the onion's skin, to continue the analogy) will still be a torus, but may not be differentiable. We have computed the rotation number for the standard map orbit shown in the right panel Fig. 4 using quadruple precision. Its 30 digit value is given in Table 1.

The forced Van der Pol oscillator. Fig. 6 shows orbits for the time- $2\pi/0.83$ map of the following periodically forced Van der Pol oscillator with nonlinear damping [23]

$$\frac{d^2x}{dt^2} - 0.2(1-x^2)\frac{dx}{dt} + 20x^3 = F \sin(0.83t), \quad (13)$$

with a variety of choices of F . While the innermost orbit shown is a chaotic attractor, the outer orbits are topological circles with quasiperiodic behavior[†]. Our computed the rotation number for the three orbits $F = 15, 25, 35$ are given in Table 1.

A two-dimensional torus map. We now introduce an example of a two-dimensional quasiperiodic torus map on \mathbb{T}^2 . This is a two-dimensional version of Arnold's family of 1D maps (see [24]), originally introduced in the following two papers [25, 26]. The map is given by (T_1, T_2) where

$$\begin{aligned} T_1(x, y) &= \left[x + \omega_1 + \frac{\epsilon}{2\pi} P_1(x, y) \right] \pmod{1} \\ T_2(x, y) &= \left[y + \omega_2 + \frac{\epsilon}{2\pi} P_2(x, y) \right] \pmod{1}, \end{aligned}$$

[†]As with the standard map, we have specified all non-essential parameters rather than stating the most general form of the Van der Pol equation.

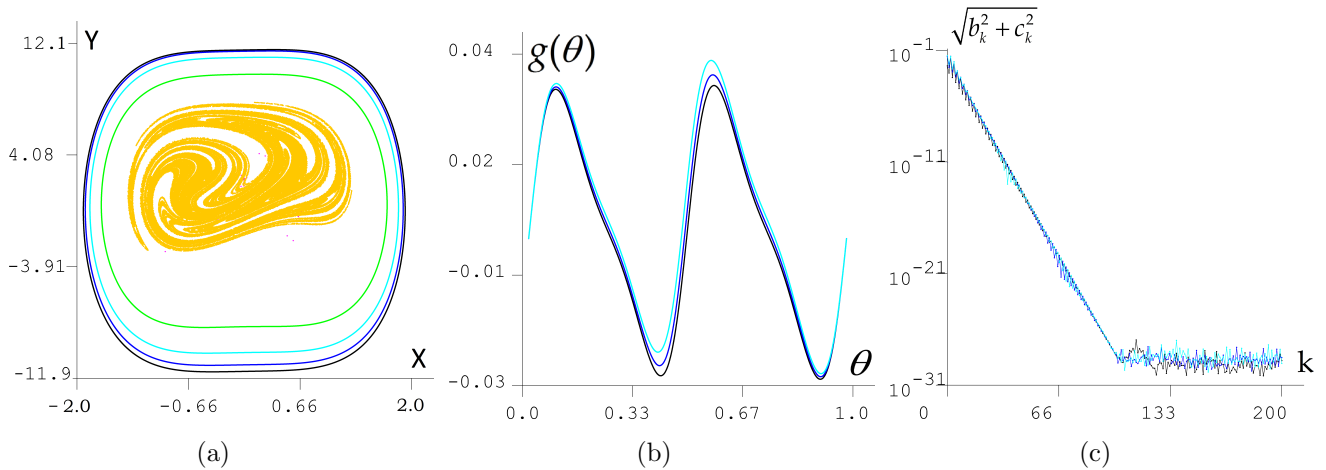


Figure 6: **Forced van der Pol oscillator.** Part (a): Attracting orbits for a number of different forcing values F for the stroboscopic map of the van der Pol flow given in (13). The plot depicts points $(X, Y) = (x(t_k), x'(t_k))$, where $t_k = 2k\pi/0.83, k = 0, 1, 2, \dots$. The chaotic orbit lying inside the cycles corresponds to $F = 45.0$. There are stable quasiperiodic orbits shown as circles, which from outermost to innermost correspond to $F = 5.0, 15.0, 25.0$ and 35.0 respectively. Part (b): the periodic part $g(\theta)$ of the conjugacy (Eq. 4) to a pure rotation, for $F = 5, 15$ and 25 . Part (c): the second figure gives a demonstration of the analyticity of the conjugacy to a pure rotation by studying the decay of the norm of the k -th Fourier coefficients with k , up to the resolution of the numerics.

and $P_i(x, y), i = 1, 2$ are periodic functions with period one in both variables, defined by:

$$P_i(x, y) = \sum_{j=1}^4 a_{i,j} \sin(2\pi\alpha_{i,j}), \text{ with } \alpha_{i,j} = r_j x + s_j y + b_{i,j}.$$

The values of all coefficients are given in Table 2. This choice of this function is based on [25, 26]. Both papers use the same form of equation, though the constants are close to but not precisely the same as the ones used previously. This is fitting with the point of view advocated in by these papers, in that the constants should be randomly chosen. Since we are using higher precision, we have chosen constants that are irrational to the level of our precision. The forward orbit is dense on the torus, and the map is a nonlinear which exhibits two-dimensional quasiperiodic behavior.

Fig. 7a depicts iterates of the orbit, indicating that it is dense in the torus. In order to verify that this map is indeed quasiperiodic, we used a Birkhoff average to compute the two Lyapunov exponents to verify that both are zero (*cf.* Fig. 7b). In terms of method, this is just a matter of changing the function f used in WB_N in Eq. 7. Likewise, finding rotation numbers in two dimensions uses the same technique as in the one-dimensional case (*cf.* Fig. 7c). In all of our calculations, the computation is significantly longer than in one dimension in order to get the same accuracy, perhaps because in two dimensions, coverage of dense orbit varies like the square of the side length of the domain.

Convergence rate. In order to explain why the convergence of our method is so good, we introduce four different possible values for the weighting function w , depicted in Fig. 8a, and compare the convergence results for computing the rotation number for each of these choices of w .

$$w_{equal}(t) = 1 \text{ (Birkhoff's choice)} \quad (14)$$

$$w_{quad}(t) = t(1-t) \quad (15)$$

$$w_{(\sin^2)}(t) = \sin^2(\pi t) \quad (16)$$

$$w_{exp}(t) = \exp(-1/(t(1-t))). \quad (17)$$

Coefficient	Value
ϵ	0.4234823
ω_1	0.71151134457776362264681206697006238
ω_2	0.87735009811261456100917086672849971
$a_{1,j}$	(-0.268, -0.9106, 0.3, -0.04)
$a_{2,j}$	(0.08, -0.56, 0.947, -0.4003)
$b_{1,j}$	(0.985, 0.0504, 0.947, 0.2334)
$b_{2,j}$	(0.99, 0.33, 0.29, 0.155)
r_j	(1, 0, 1, 0)
s_j	(0, 1, 1, -1)
Computed ρ_1	0.718053759982066107095244936117
Computed ρ_2	0.885304666596099792113366824157

Table 2: **Coefficients for the torus map.** All values are used in quadruple precision, but in this table the repeated zeros on the end of the number are suppressed.

If we compute with the first choice of w , we recover the a truncated series in the definition of the Birkhoff average. To estimate the error, we expect the difference $f(x_{N+1}) - f(x_N)$ to be of order one, implying that

$$\text{WB}_{w_{\text{equal}}, N+1} - \text{WB}_{w_{\text{equal}}, N} \sim 1/N.$$

The choice of a particular starting point also creates a similar uncertainty of order $1/N$. For all but the first choice, w is always positive between 0 and 1 but vanishes as t approaches 0 and 1. In addition, going down the list, increasing number of derivatives of w vanish for $t \rightarrow 0$ and $t \rightarrow 1$, with all derivatives of w_{exp} vanishing at 0 and 1. We thus expect the effect of the starting and endpoints to decay at the same rate as this number of vanishing derivatives. Indeed, we find that w_{quad} corresponds approximately to order $1/N^2$ convergence, $w_{(\sin^2)}$ to $1/N^3$ convergence, and w_{exp} to convergence faster than any polynomial. Figs. 8b and 7bc show this effect.

Related methods. See [4, 5] for references to earlier methods for computing rotation numbers. In [4, 5], A. Luque and J. Villanueva develop fast methods for obtaining rotation numbers for analytic functions on a quasiperiodic torus, sometimes with quasiperiodic forcing with several rotation numbers. The paper [5] examines a smooth function f on a quasiperiodic torus. Let f_n denote the value of f at the n -th trajectory point. From this sequence they can obtain the rotation number with error satisfying $|\text{error}| \leq C_p N^{-p}$ for any p where C_p is a constant. The method of computation depends on p and as p increases the computational complexity increases for fixed N . If $T(p, N)$ is their computation time, it appears that $T(p, N)/N \rightarrow \infty$ as $p \rightarrow \infty$. In comparison, computation time for our weighted Birkhoff average is simply proportional to N since it requires a sum of N numbers. The paper gives one figure (Fig 6) from which the rate of convergence can be computed, namely a restricted three-body problem. Their rotation-rate error is proportional to $N^{-3.5}$ and is $\approx 10^{-18}$ at $N = 2^{21}$.

Several variants of the Newton's method have been employed to determine quasiperiodic trajectories in different settings. In [27] the monodromy variant of Newtons method was applied to locate periodic or quasi-periodic relative satellite motion. A PDE-based approach was taken in [28], where the authors defined an invariance equation which involves partial derivatives. The invariant tori are then computed using finite element methods. See also Chapter 2, [28] for more references on the numerical computation of invariant tori.

3.2 Fourier coefficients and conjugacy reconstruction

For a quasiperiodic curve as shown in Fig. 3a, there are two approaches to representing the curve. Firstly, we can write the coordinates (X, Y) as a function of $\theta \in S^1$, or secondly, we can reduce the dimension and represent the points on the curve by an angle $\phi \in S^1$, that is, $\phi(X(\theta), Y(\theta))$, which is also $h(\theta) = \theta + g(\theta)$. We have shown g in Fig 3b and the exponential decay of the norm of the Fourier coefficients in Fig. 3c. To limit the number of graphs in this paper, we have only created the Fourier series for the periodic part $g(\theta)$

Given a continuous periodic map $f : S^1 \rightarrow \mathbb{R}$, where S^1 is a circle (or one-torus), the Fourier sine and cosine representation of f is the following.

$$\text{For every } t \in S^1, f(t) = \frac{b_0}{2} + \sum_{k=1}^{\infty} b_k \cos(2k\pi t) + \sum_{k=0}^{\infty} c_k \sin(2k\pi t) \quad (18)$$

where the coefficients b_k and c_k are given by the following formulas.

$$b_k = 2 \int_{\theta \in S^1} f(\theta) \cos(2k\pi\theta) d\theta, \quad (19)$$

$$c_k = 2 \int_{\theta \in S^1} f(\theta) \sin(2k\pi\theta) d\theta. \quad (20)$$

To be able to use the fast Fourier transform, 2^M equally spaced points on the circle are required. If we only have access to an ergodic orbit (x_n) on the circle, then we cannot use the fast Fourier transform as we only have the function values $f(x_n)$ along a quasiperiodic trajectory, and a rotation number ρ . So instead, we obtain these coefficients using a weighted Birkhoff average on a trajectory (x_n) by applying the functional $\text{WB}_{w,N}$. For $k = 0$, we find a_0 by applying WB to the function 1. For $k > 0$, we find b_k and c_k as follows.

$$b_k = \text{WB}_{w,N}(f(\theta) \cos(2k\pi\theta)) = \sum_{n=0}^N f(x_n) \cos(2k\pi n\rho) \hat{w}_{n,N}. \quad (21)$$

$$c_k = \text{WB}_{w,N}(f(\theta) \sin(2k\pi\theta)) = \sum_{n=0}^N f(x_n) \sin(2k\pi n\rho) \hat{w}_{n,N}. \quad (22)$$

By specifying that $\theta_0 = 0$, our computation of rotation number ρ provides all iterates : $\theta_n = n\rho$. Using the Fourier coefficients, we can thus reconstruct the periodic part of the change of variables function g (see Eq. 5). This is depicted for the restricted three-body problem in Fig. 3, for the standard map in Fig. 5, for the forced van der Pol equation in Fig. 6. In all three one-dimensional cases, we depict $\sqrt{b_k^2 + c_k^2}$ as a function of k . Our main observation is that the Fourier coefficients decay exponentially; that is, for some positive numbers α and β , in dimension one, the Fourier coefficients b_k and c_k satisfy

$$\sqrt{|b_k|^2 + |c_k|^2} \leq \alpha e^{-\beta|k|} \text{ for all } k \in \mathbb{Z}. \quad (23)$$

This is characteristic of analytic functions. We therefore state that all of the conjugacy functions that we computed in our examples are effectively analytic, “effectively” meaning within the precision of our quadruple precision numerics.

In two dimensions, the computation of Fourier coefficients is similar, but instead of only having one set of cosine and sine functions, for each (j, k) , we have two linearly independent sets of complex-valued functions, where $i = \sqrt{-1}$:

$$e^{i(jx+ky)} \text{ and } e^{i(jx-ky)}.$$

We define $a_{j,k}$ and $b_{j,k}$ to be the complex-valued coefficients corresponding to each of these functions. The reconstructed conjugacy function and decay of coefficients for the two-dimensional torus is depicted in

Fig. 9. The decay of coefficients shows $\sqrt{j^2 + k^2}$ on the horizontal axis, and $|b_{j,k}|$ and $|c_{j,k}|$ on the vertical axis, where both of these coefficients are complex, meaning that $|\cdot|$ represents the modulus. Again here, the coefficients decay exponentially, though the decay of coefficients is considerable slower in two dimensions due to the added dimension. The data looks quite a lot more crowded in this case, since there are many different values of (j, k) such that the values of $\sqrt{j^2 + k^2}$ are identical or very close. In addition, the two sets of coefficients $b_{j,k}$ and $c_{j,k}$ generally converge at different exponential rates. This is why there is a strange looking set of two different clouds of data in Fig. 9b. While more information on the difference between these coefficients is gained by interactively viewing the data in three dimensions, we have not been able to find a satisfactory static flat projection of this data. We feel that in a still image, the data cloud shown conveys the maximum information.

Accuracy of the calculation of Fourier coefficients. Our method of calculation of the Fourier coefficients is dependent on the knowledge of the rotation vector $\vec{\rho}$, or an approximation $\hat{\vec{\rho}}$. For the rest of the chapter, $m \in \mathbb{N}$ is some fixed integer and M is some integer satisfying $M > d + m(d + \beta)$, where β is the Diophantine class of $\vec{\rho}$. Let $\Delta\vec{\rho}$ be the error in the approximation of ρ , that is,

$$\Delta\vec{\rho} := \hat{\vec{\rho}} - \vec{\rho}.$$

We are interested in knowing how the error in the calculation of Fourier coefficients b_k, c_k depend on $\Delta\vec{\rho}$. Let for every $k \in \mathbb{Z}^d$, $\mathbf{f}_k(\theta) := e^{i2\pi k \cdot \theta}$. Then every periodic function g has the complex Fourier series representation

$$g(\theta) = \sum_{k \in \mathbb{Z}^d} a_k f_k, \text{ where } a_k = \int_{\mathbb{T}^d} g(\theta) f_{-k}(\theta)$$

Therefore, a_k can be approximated as

$$\hat{a}_k = \text{WB}_{N, \hat{\vec{\rho}}}(g(\theta) f_{-k}(\theta)) = \sum_{n=0}^{N-1} g(n\vec{\rho}) e^{-i2\pi n k \cdot \hat{\vec{\rho}}} \hat{w}_{n,N}.$$

Corollary 3.1 *If $N\|k \cdot \Delta\vec{\rho}\| \ll 1$, then for each $m \in \mathbb{N}$, there exists a constant $C_{g,w,m} > 0$ such that*

$$\frac{|\hat{a}_k(g) - a_k(g)|}{|a_k(g)|} \leq \pi N \|k \cdot \Delta\vec{\rho}\| + C_{g,w,m} N^{-m}.$$

Proof We begin by obtaining bounds on the error in calculating the Fourier coefficients of pure exponentials. Note that $a_k(f_l)$ equals 1 if $l = k$, equals 0 if $l \neq k$. We will estimate the error $|\hat{a}_k(f_l) - a_k(f_l)|$ in each case.

$$|\hat{a}_k(f_k) - a_k(f_k)| = |\text{WB}_{N, \hat{\vec{\rho}}}(f_k(\theta) f_{-k}(\theta)) - 1| = \left| \sum_{n=0}^{N-1} e^{-i2\pi n k \cdot \Delta\vec{\rho}} \hat{w}_{n,N} - 1 \right|.$$

Then if $N\|k \cdot \Delta\vec{\rho}\| \ll 1$, then using the approximation $e^{i\alpha} - 1 \approx i\alpha$, one can say that

$$\begin{aligned} |\hat{a}_k(f_k) - a_k(f_k)| &= |\hat{a}_k(f_k) - 1| \\ &= \left| \sum_{n=0}^{N-1} (e^{-i2\pi n k \cdot \Delta\vec{\rho}} - 1) \hat{w}_{n,N} \right| \\ &\leq \sum_{n=0}^{N-1} |e^{-i2\pi n k \cdot \Delta\vec{\rho}} - 1| \hat{w}_{n,N} \\ &\leq \sum_{n=0}^{N-1} 2\pi n k \cdot |\Delta\vec{\rho}| \hat{w}_{n,N} \\ &= \pi N \|k \cdot \Delta\vec{\rho}\|. \end{aligned}$$

Since $\vec{\rho}$ is Diophantine with Diophantine class $\beta \geq 0$, for every $\alpha \in \mathbb{R}$, there exists a constant $C_{\vec{\rho}} > 0$ such that for all $l \in \mathbb{Z}^d$ with $\|l\|$ sufficiently big, one has

$$|\exp(i2\pi(l \cdot \vec{\rho} - \alpha) - 1)| = |\exp(i2\pi(l \cdot \vec{\rho} - \alpha) - \exp(i2\pi\alpha))| \geq C_{\vec{\rho}} \|l\|^{-(d+\beta)} \quad (24)$$

By Eq. 14 from [3], for every $l \neq k$ there exists a constant $C_{w,m} > 0$ depending on w and m such that for every $\alpha \in \mathbb{R}$

$$\left| \sum_{n=0}^{N-1} \exp(-i2\pi n\alpha) \hat{w}_{m,N} \right| \leq C_{w,m} N^{-m} |e^{i2\pi\alpha} - 1|^{-m} \quad (25)$$

Combining Eqs. 24 and 25, we get

$$\begin{aligned} |\hat{a}_k(f_l) - a_k(f_l)| &= |\hat{a}_k(f_l)| \\ &= \left| \sum_{n=0}^{N-1} \exp(-i2\pi n(l \cdot \vec{\rho} - k \cdot \hat{\rho})) \hat{w}_{m,N} \right| \\ &\leq C_{w,m} N^{-m} |\exp(i2\pi(l \cdot \vec{\rho} - k \cdot \hat{\rho})) - 1|^{-m} \\ &\leq C_{w,m} C_{\vec{\rho}} N^{-m} \|l\|^{m(d+\beta)} \end{aligned}$$

Since $f \in C^M$, there exists $C_{g,M} > 0$ depending on g and M such that for each $l \neq \vec{0}$, $|a_l| \leq C_{f,M} \|l\|^{-M}$. Therefore, in a manner similar to the derivation of Eq. 15 from [3], we can write

$$\begin{aligned} |\hat{a}_k(g) - a_k(g)| &= \left| \sum_{l \in \mathbb{Z}^d} a_l (a_k(f_l) - a_k(f_l)) \right| \\ &\leq |a_k(a_k(f_k) - a_k(f_k))| + \left| \sum_{l \neq k} a_l (a_k(f_l) - a_k(f_l)) \right| \\ &\leq |a_k| \pi N |k \cdot \Delta \vec{\rho}| + \sum_{l \neq k} |a_l (a_k(f_l) - a_k(f_l))| \\ &\leq |a_k| \pi N |k \cdot \Delta \vec{\rho}| + C_{w,m} C_{\vec{\rho}} N^{-m} \sum_{l \neq k} |a_l| \|l\|^{m(d+\beta)} \\ &\leq |a_k| \pi N |k \cdot \Delta \vec{\rho}| + C_{w,m} C_{\vec{\rho}} C_{f,M} N^{-m} \sum_{l \neq k} \|l\|^{-M} \|l\|^{m(d+\beta)} \\ &= |a_k| \pi N |k \cdot \Delta \vec{\rho}| + C_{w,m} C_{\vec{\rho}} C_{f,M} N^{-m} \sum_{l \neq k} \|l\|^{-(M-m(d+\beta))} \end{aligned}$$

Since $M > d + m(d + \beta)$, the sum $\sum_{l \neq k} \|l\|^{-(M-m(d+\beta))} < \infty$. The statement of the corollary now follows. ■

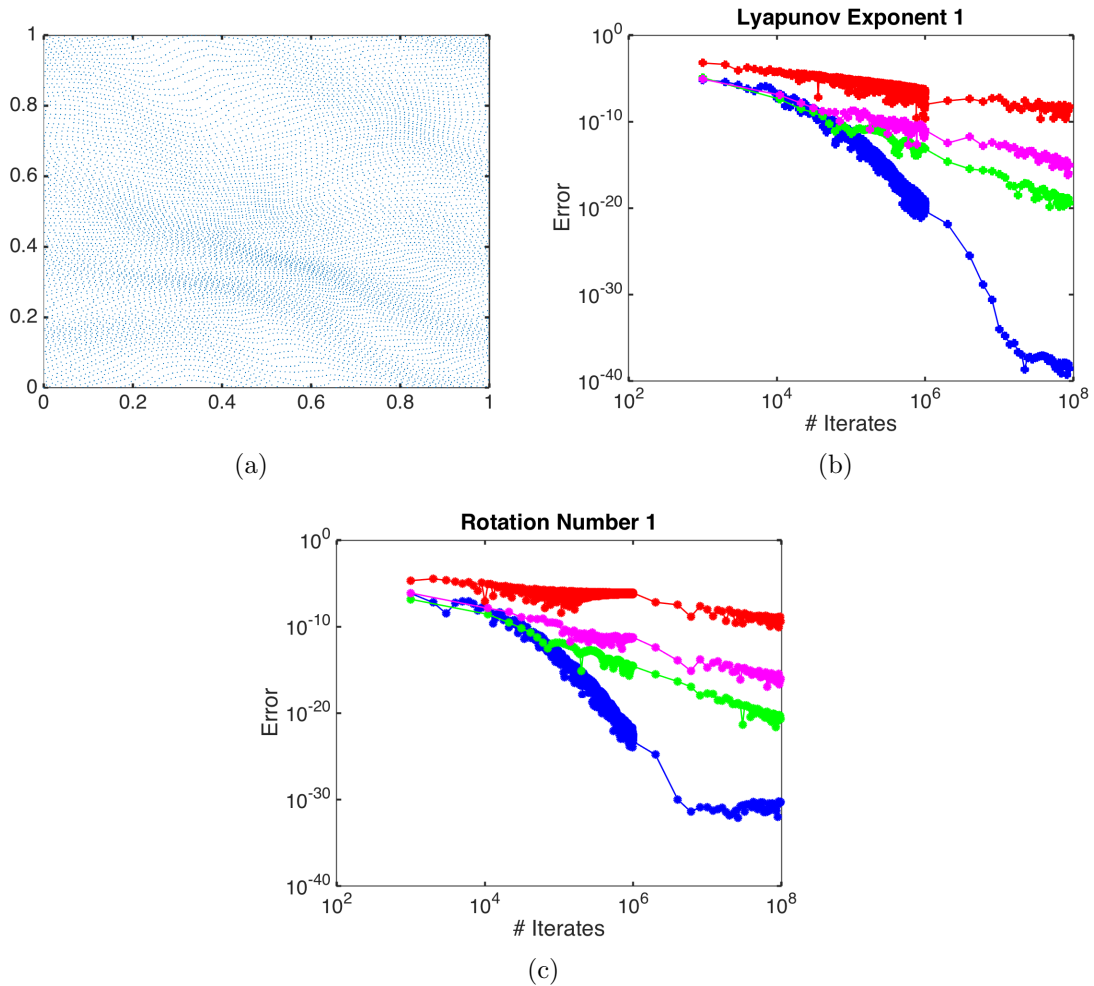


Figure 7: **Two-dimensional torus map.** Fig. (a) shows the first 10^4 iterates of an orbit for the two-dimensional quasiperiodic torus map. The orbit appears to be dense, indicating quasiperiodicity. This is confirmed by computing the two Lyapunov exponents of the orbit using Birkhoff averaging and finding them to be 0. The convergence of this computation for one of the two Lyapunov exponents is shown in blue in (b). The highest to lowest curves show the convergence rates resp. for the first three weighting functions given in (14). Fig. (c) shows the convergence rate for the first rotation number for the four different weighting functions.

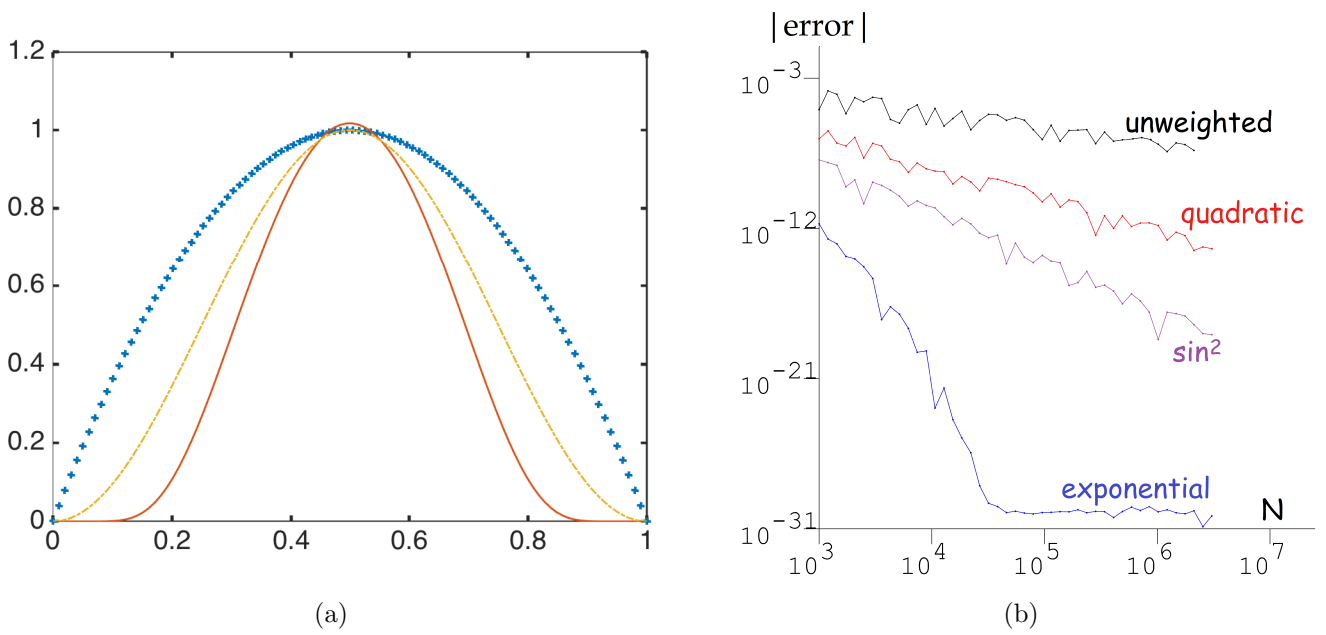


Figure 8: **Rate of convergence for different weight functions.** Left is a plot of the three non-constant weighting functions from (14) (quad blue, \sin^2 yellow, exp red). Since only the shape matters, they have been rescaled so that each has a peak of approximately one. For a given w and a given number of iterates N , the rotation number $\hat{\rho}$ approximation is calculated for B_1 of the restricted three-body problem, the error of the calculation is the difference $|\rho - \hat{\rho}|$. The figure shows the convergence rate of this error as a function of N . The exponential weight function is seen to be the best method. The error cannot be reduced below 10^{-32} because that is the limit of quadruple precision.

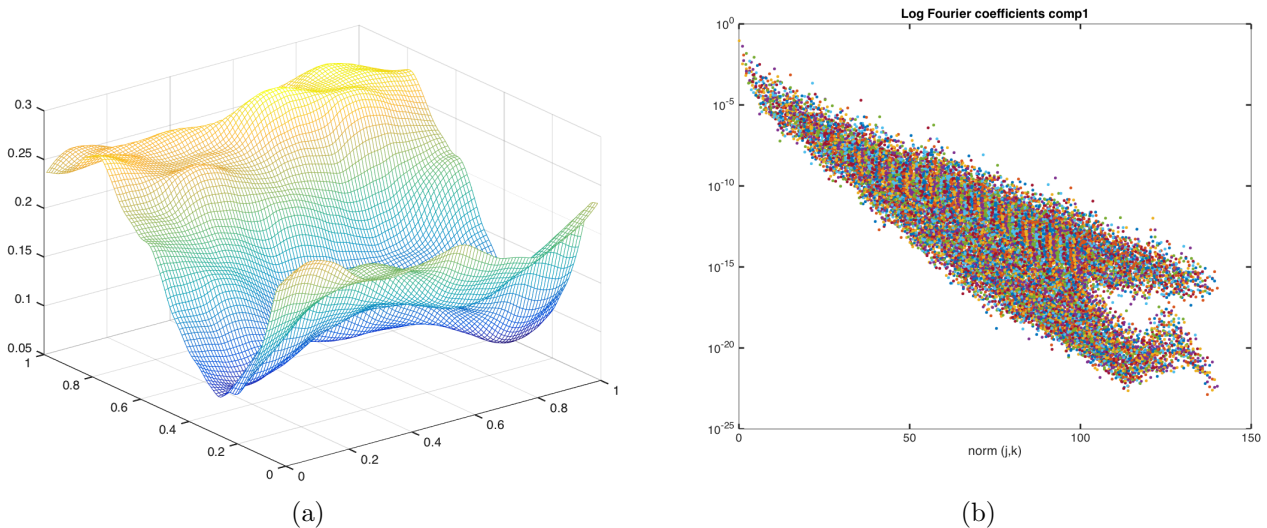


Figure 9: **Conjugacy for the torus.** Fig. (a) depicts the reconstruction of the periodic part g (see 5) of the first component of the conjugacy function for the torus map. The second conjugacy function is similar but not depicted here. Fig. (b) shows the decay of the Fourier coefficients for this component of the conjugacy function on the log-linear scale.

References

- [1] E Sander and J A Yorke. The many facets of chaos. *International Journal of Bifurcation and Chaos*, 25(4):15300, 2015.
- [2] S Newhouse, D Ruelle, and F Takens. Occurrence of strange Axiom A attractors near quasiperiodic flows on T^m , $m \geq 3$. *Comm. Math. Phys.*, 64(1):35–40, 1978/79.
- [3] S Das and J A Yorke. Super convergence of ergodic averages for quasiperiodic orbits. *Preprint*, 2015.
- [4] T M Seara and J Villanueva. On the numerical computation of Diophantine rotation numbers of analytic circle maps. *Phys. D*, 217(2):107–120, 2006.
- [5] A Luque and J Villanueva. Quasi-periodic frequency analysis using averaging-extrapolation methods. *SIAM J. Appl. Dyn. Syst.*, 13(1):1–46, 2014.
- [6] C Simó. *Averaging under fast quasiperiodic forcing*. Plenum Pub. Co., New York, 1994.
- [7] C Simó, P Sousa-Silva, and M Terra. Practical stability domains near $L_{4,5}$ in the restricted three-body problem: Some preliminary facts. *Progress and Challenges in Dynamical Systems*, 54:367–382, 2013.
- [8] F Durand and D Schneider. Ergodic averages with deterministic weights. *Annales de l'institut Fourier*, 2002.
- [9] C Baesens, J Guckenheimer, Seunghwan Kim, and R S MacKay. Three coupled oscillators, 1990.
- [10] H W Broer and G B Huitema. Unfoldings of Quasi-periodic Tori in Reversible Systems, 1993.
- [11] R Vitolo, H Broer, and C Simó. Quasi-periodic bifurcations of invariant circles in low-dimensional dissipative dynamical systems. *Regular And Chaotic Dynamics*, 16(1-2):154–184, February 2011.
- [12] H Hanßmann and C Simó. Dynamical stability of quasi-periodic response solutions in planar conservative systems. *Indagationes Mathematicae*, 23(3):151–166, September 2012.
- [13] M B Sevryuk. Quasi-periodic perturbations within the reversible context 2 in KAM theory. *Indagationes Mathematicae*, 23(3):137–150, September 2012.
- [14] H W Broer, G B Huitema, F Takens, and B L J Braaksma. Unfoldings and bifurcations of quasi-periodic tori. *Memoirs of the American Mathematical Society*, 83(421):viii–175, 1990.
- [15] A P Kuznetsov, N A Migunova, I R Sataev, Y V Sedova, and L V Turukina. From chaos to quasi-periodicity. *Regular And Chaotic Dynamics*, 20(2):189–204, May 2015.
- [16] H Poincaré. *Leons de mécanique céleste : professées à la Sorbonne*. Paris : Gauthier-Villars, 1905.
- [17] J B Greene. *Poincaré and the Three Body Problem*. American Mathematical Society, October 29, 1996.
- [18] N G Markley. Transitive homeomorphisms of the circle. *Mathematical systems theory*, 2 (3):247–249, 1968.
- [19] E R Van Kampen. The topological transformations of a simple closed curve into itself. *American Journal of Mathematics*, 57 (1):142–152, January, 1935.

- [20] M R Herman. Sur la conjugaison différentiable des difféomorphismes du cercle des rotations. *Publications Mathématiques de l'Institut des Hautes études Scientifiques*, 49 (1):5–233, 1979.
- [21] Y Yamaguchi and K Tanikawa. A remark on the smoothness of critical KAM curves in the standard mapping. *Progress of Theoretical Physics*, 101 (1), January, 1999.
- [22] S N Chow, M van Noort, and Y Yi. Quasiperiodic dynamics in Hamiltonian 1.5 degree of freedom systems far from integrability. *Journal of Differential Equations*, 212:366–393, 2005.
- [23] B van der Pol. A theory of the amplitude of free and forced triode vibrations. *Radio Review*, 1:701–710, 1920.
- [24] V Arnold. Small denominators. i. mapping of the circumference onto itself. *Amer. Math. Soc. Transl. (2)*, 46:213–284, 1965.
- [25] C Grebogi, E Ott, and J A Yorke. Are three-frequency quasiperiodic orbits to be expected in typical nonlinear dynamical systems? *Physical Review Letters*, 51(5):339, 1983.
- [26] C Grebogi, E Ott, and J A Yorke. Attractors on an N-torus: Quasiperiodicity versus chaos. *Physica D. Nonlinear Phenomena*, 15(3):354–373, April 1985.
- [27] V M Becerra, J D Biggs, S J Nasuto, V F Ruiz, W Holderbaum, and D Izzo. Using Newton's method to search for quasi-periodic relative satellite motion based on nonlinear Hamiltonian models. *7th International Conference On Dynamics and Control of Systems and Structures in Space*, 7, 2006.
- [28] F Schilder, H M Osinga, and W Vogt. Continuation of quasi-periodic invariant tori. *SIAM Journal on Applied Dynamical Systems*, 4 (3):459–488, 2005.